Chapter 5
Electrochemical Characterization of Photocatalytic Materials

Erika Bustos, Juan Manríquez, Juan Manuel Peralta-Hernández, and Edgar J. Ruiz-Ruiz

Abstract The semiconductor–electrolyte interface have interesting similarities and differences with their semiconductor–metal (or metal oxide) and metal–electrolyte counterparts. Thus, approaches to garnering a fundamental understanding of these interfaces have stemmed from both electrochemistry and solid-state physics perspectives and have proven to be equally fruitful. Electron transfer theories were also rapidly evolving during this period, starting from homogeneous systems to heterogeneous metal–electrolyte interfaces leading, in turn, to semiconductor–electrolyte junctions.

To facilitate a self-contained description, this chapter will start with well-established aspects related to the thermodynamic properties as semiconductor energy band model and the electrostatics at semiconductor–electrolyte interfaces in the dark. Additionally, this chapter examines the kinetic properties in the processes of light absorption, electron–hole generation, and charge separation at these interfaces. The steady state and dynamic aspects of charge transfer are then briefly considered. Nanocrystalline semiconductor films and size quantization are then discussed as are issues related to electron transfer across chemically modified semiconductor–electrolyte interfaces to determine the photocatalytic efficiency of semiconductor materials.

E. Bustos (✉) • J. Manríquez
Centro de Investigación y Desarrollo Tecnológico en Electroquímica, S. C., Parque Tecnológico Querétaro s/n, Sanfandila, Pedro Escobedo, 76703 Querétaro, Qro., México
e-mail: ebustos@cideteq.mx

J.M. Peralta-Hernández
Centro de Innovación Aplicada a Tecnologías Competitivas, A. C., Calle Omega No. 201 - Fracc. Ind. Delta, 37545 León, Gto., México

E.J. Ruiz-Ruiz
Universidad Autónoma de Nuevo León, Facultad de Ciencias Químicas, Av. Pedro de Alba, Ciudad Universitaria, San Nicolás de los Garza, Nuevo León, México

A. Hernández-Ramírez, I. Medina-Ramírez (eds.), *Photocatalytic Semiconductors*,
DOI 10.1007/978-3-319-10999-2_5

Table 5.1 Common semiconductors used as photoanodes

Semiconductor	Conductivity type (s)	Optical band gap energy (eV)
Si	*n*,*p*	1.11
InP	*n*,*p*	1.35
GaAs	*n*,*p*	1.42
CdTe	*n*,*p*	1.50
CdSe	*n*	1.70
α-Fe_2O_3	*n*	2.20
GaP	*n*,*p*	2.26
$BiVO_4$	*n*	2.40
CdS	*n*	2.5
WO_3	*n*	2.80
TiO_2	*n*	3.00 (rutile)
		3.20 (anatase)
$SrTiO_3$	*n*	3.2
ZnO	*n*	3.35
SnO_2	*n*	3.8

5.1 Characterization of Thermodynamic Properties in the Semiconductor–Electrolyte Interface Using Electrochemical Techniques

5.1.1 The Double Layer at Semiconductor

Electrodes prepared with a photocatalytic semiconductor can be used in a photoelectrochemical cell to measure its properties including the band gap energy, flat-band potential, and kinetics of hole and electron transfer.

The semiconductor must be supported on an electronic conductor substrate and put it into an electrochemical cell in contact with electrolytic solution. Since in a photoelectrode the electron transfer occurs necessarily at the interface between the semiconducting photoanode and the electrolyte, first, an explanation about the semiconductor–electrolyte interface is important. The band bending is a result of interface phenomena and the characteristic charge transfer reactions across the solid electrolyte that represents the basis of an electrode. Table 5.1 shows the most common semiconductors used as photoanodes (Rajeshwar 2002, Souza et al. 2009, Serpone and Pellizeti 1989).

The interface of semiconductor electrodes is described as either in the state of band edge level pinning or in the state of Fermi level pinning (Sato 1998). After the contact of the semiconductor surface with the electrolyte, the thermodynamic equilibrium on both sides of the interface must be established (Beranek 2011).

The charge distribution at semiconductor–electrolyte interface is summarized in Fig. 5.1. Three distinct double layers can be distinguished at the interface.

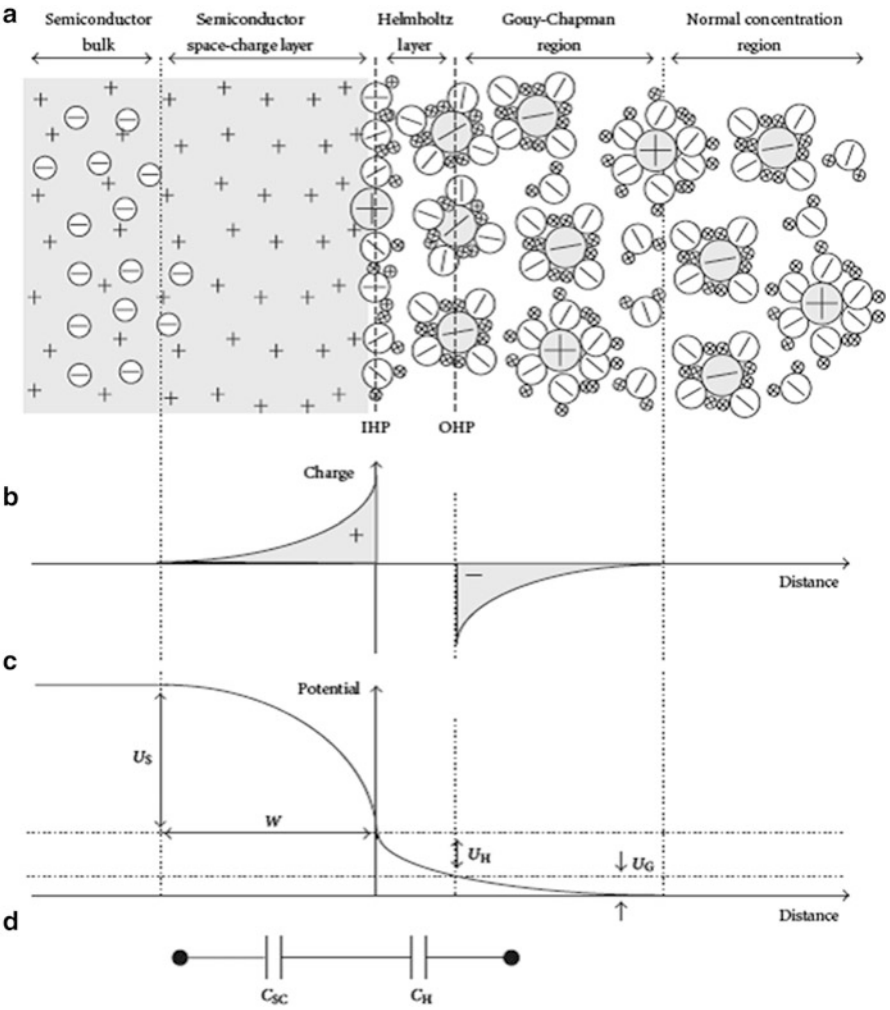

Fig. 5.1 Schematic view of the electric double layers at the n-type semiconductor–aqueous electrolyte interface (**a**) with corresponding charge (**b**) and potential (**b**) distributions. U_S is the potential drop across the space-charge layer, U_H is the potential drop in the Helmholtz layer, and U_G represents the drop in the Gouy–Chapman layer; (**d**) the equivalent circuit for the interface assuming that U_G can be neglected. From reference Beranek (2011)

First, is the semiconductor space-charge layer with positive charges in the form of ionized donors and the counter negative charge located at the surface. The second one is the Helmholtz double layer consisting of the inner Helmholtz plane (IHP) located at the semiconductor surface, and the charge is in the surface states or at the location of specifically adsorbed ions, whereas the latter denotes the position of the closest approach of hydrated mobile ions and the outer Helmholtz plane (OHP).

The third double layer is the Gouy–Chapman layer which is an extended region with an excess of free ions of one sign.

Essentially, the double layers act as parallel-plate capacitors connected in series with capacitances C_{SC}, C_H, and C_G representing the capacitance of the space-charge layer, the capacitance of the Helmholtz double layer, and the capacitance of the Gouy–Chapman layer, respectively, whereby C_G can be typically neglected for electrolytes containing relatively high concentrations of redox species (Fig. 5.1d) (Sato 1998). The thickness of the diffuse layer depends on the total ionic concentration in the solution; for concentrations greater than 10 ~ 2 M, the thickness is less than ~100 A (Bard and Faulkner 2000).

The space-charge region formed at the interface provides a strong electric field that is indispensable for an effective separation of photoexcited electrons from holes. On the other hand, when light is absorbed in the bulk of the photoanode, the photoexcited electrons and holes are created, but there is a high probability they will recombine before being used for water photolysis. Therefore, if light is absorbed in this region, a charge separation and field-assisted transport are expected (Radecka et al. 2008).

The band bending is also affected by the external voltage V_B. For a given semiconductor and electrolyte, there exists a unique potential for which the potential drop between the surface and the bulk is zero and there is no space-charge layer. This is the flat-band potential V_{Fb} or, in other words, is the applied potential (V) at which the semiconductor energy bands are "flat" leading up the solution junction. For an *n*-doped semiconductor, the flat-band potential is rather close to the conduction band edge, and experimentally the two concepts are sometimes treated as interchangeable (Jacobsson and Edvinsson 2012).

5.1.2 The Flat-Band Potential

There exist some electrochemical methods to determine the flat-band potential. The two most common methods are described as follows: the first one stems from the impedance spectroscopy in the dark, and the second one employs the current–voltage characteristics under a light pulse. The flat-band potential of *p*-type electrode is more anodic (positive) than that of *n*-type electrode; this difference in the flat-band potential between the two types of the same semiconductor electrode is nearly equivalent to the band gap of the semiconductor (Lee et al. 2001).

Considerations of interfacial electron transfer require knowledge of the relative positions of the participating energy levels in the two (semiconductor and solution) phases. Models for redox energy levels in solution have been exhaustively treated elsewhere. Besides the Fermi level of the redox system, the thermal fluctuation model (Kuhn-Kuhnenfeld 1972) leads to a Gaussian distribution of the energy levels for the occupied (reduced species) and the empty (oxidized species) states, respectively.

The distribution functions for the states to oxidation (D_{ox}) and reduction (D_{red}) are given by Eqs. (5.1) and (5.2), where E is the cell potential, $E_{F,redox}$ is the Fermi redox potential, λ is the solvent reorganization energy, k_B is Boltzmann's constant, and T is the temperature in Kelvin:

$$D_{ox} = \exp\left[-\frac{E - E_{F,redox} - \lambda^2}{4\,k_B T\lambda}\right] \tag{5.1}$$

$$D_{red} = \exp\left[-\frac{E - E_{F,redox} + \lambda^2}{4\,k_B T\lambda}\right] \tag{5.2}$$

Now consider the relative disposition of these solution energy levels with respect to the semiconductor band edge positions at the interface. The total potential difference across this interface is given by Eq. (5.3) (Rajeshwar 2002):

$$V_t = V_{SC} + V_H + V_G \tag{5.3}$$

In the last equation, V_t is the potential as measured between an ohmic contact on the rear surface of the semiconductor electrode and the reference electrode. The problematic factors in placing the semiconductor and solution energy levels on a common basis involve V_H and V_G, where V_H is the potential drop in the Helmholtz layer and V_G represents the drop in the Gouy–Chapman layer potential. In other words, theoretical predictions of the magnitude of the space-charge layer potential V_{SC} (and how it changes as the redox couple is varied) are hampered by the lack of knowledge on the magnitude of V_H and V_G. A degree of simplification is afforded by employing relatively concentrated electrolytes such that V_G can be ignored. As with metals, the Helmholtz layer is developed by adsorption of ions or molecules on the semiconductor surface, by oriented dipoles, or especially in the case of oxides, by the formation of surface bonds between the solid surface and species in solution. Recourse to band edge placement can be sought through differential capacitance measurements on the semiconductor–redox electrolyte interface (Takahashi 1979, Tenne and Hodes 1980).

Once V_{Fb} is known (from measurements), the Fermi level of the semiconductor at the surface is defined. It is then a simple matter to place the energies corresponding to the conduction and V_B at the surface (E_{CB} and E_{VB}, respectively) if the relevant doping levels are known. The difference between E_{CB} and E_{VB} should approximately correspond to the semiconductor band gap energy, E_g. Alternatively, if V_{Fb} is measured for one given state of doping of the semiconductor (n or p doped), the other band edge position can be fixed from knowledge of E_g. It is important to stress that the semiconductor surface band edge positions (as estimated from V_{Fb} measurements) comprises all the terms and reflects the situation in situ for a given set of conditions (solution pH, redox concentration, etc.) of the semiconductor redox electrolyte. The situation obviously becomes complex when the charge distribution and mediation at the interface changes either via surface states and illumination or both (Bard and Faulkner 2001).

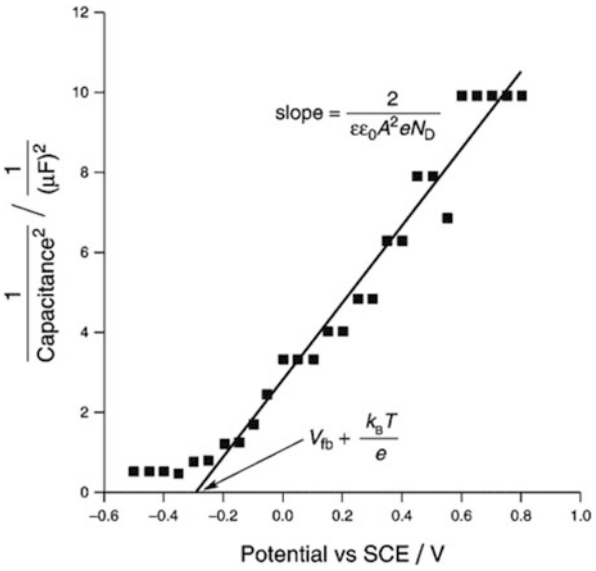

Fig. 5.2 Mott–Schottky plot of ZnO versus SCE in 7×10^{-4} M $K_3[Fe(CN)_6]$ (1 M KCl) obtained from reference Gelderman et al. (2007). Copyright 2007 American Chemical Society

In the simplest case as more fully discussed elsewhere (Takahashi 1979; Hodes et al. 1981; Tenne and Hodes 1980), one obtains the Mott–Schottky relation (for the specific instance of an *n*-type semiconductor) of the semiconductor depletion layer capacitance (C_{SC}). Mott–Schottky (MS) plots for layers over a surface of electrode can be obtained from electrochemical impedance spectroscopy (EIS) experiments at a constant frequency in aqueous medium. The resulting curves of the inverse square capacitance ($1/C^2$) versus cell potential (E) represent the classical Mott–Schottky equation (5.4). Generally, the *flat-band potential* (V_{Fb}) values are determined by measuring the capacitance of the electrode/electrolyte interface at different electrode potentials (V) using the Mott–Schottky equation, where C is the capacitance of the solid/electrolyte interface; ε_o and ε_s are the dielectric constants of free space and the film electrode, respectively; q is the electronic charge; V_{Fb} is the flat-band potential; T is the temperature in Kelvin; N_D is the donor density; V is the applied potential; and k_B is Boltzmann's constant. The V_{Fb} value and N_D can be determined from the extrapolation for $1/C^2$) (Cho et al. 2009; Manríquez and Godínez 2007):

$$\frac{1}{C^2} = \left[\left[\frac{2}{\varepsilon_o \varepsilon_s q N_D}\right]\left[(V_B V_{Fb}) - \left(\frac{k_B T}{q}\right)\right]\right] \tag{5.4}$$

At high concentration of multiple donor levels, an indirect tunneling of electrons through the semiconductor layer is promoted, causing a change in the slope (see Fig. 5.2). This change is determined by the distribution of relaxation times for electron emission depending on the position of the states related to the conduction band (Beranek 2011).

Figure 5.2 presents the flat-band potential of ZnO semiconductor versus SCE in 7×10^{-4} M $K_3[Fe(CN)_6]$ (1 M KCl) previously oxygen purged, using the Mott–Schottky plot. By linear extrapolation to "x" axe can be obtained the value of V_{Fb}; according with the graphic this value is about -0.316 ± 0.033 V for a single crystal of ZnO with a well-defined crystal plane, [001] synthesized by Gelderman et al. (2007). The N_D can be obtained from the slope in the Mott–Schottky plot, if the dielectric constants ε_s and charge are known. Then, from the slope, $N_D = 2 \times 10^{24}$ m^{-3}, which is comparable to previously reported values (6×10^{24} m^{-3}). Authors attribute this deviation due to the action of surface states in the polycrystalline electrode capturing and immobilizing the carriers. If the number of dopant agents per unit of volume of semiconductor (N_D) is minor to the effective number of accessible states at the conduction band (N_C), which means that $N_D < N_C$, then the photoactivity of the semiconductor is increased, becoming more intense the bending of the band; in this case, the semiconductor is nondegenerate. Nevertheless in case of $N_D > N_C$, the semiconductor exhibits a quasi-metallic behavior and is said to be degenerate.

5.1.3 Light Pulse Techniques

The light pulse technique (LPT) and the scanning light pulse technique (SLPT) are photoelectric methods used to determine electrical parameters of metal oxide semiconductor structures. The LPT method may be used to determine the V_{Fb} value of the entire semiconductor device, while the SLPT method allows determination of the distribution of local V_{Fb} values over the gate area. Most of the cases area is scanned by a small light beam (Piskorski and Przewlocki 2009).

Photocurrent vs. potential curves are typically obtained by applying a scan potential to the semiconductor–electrolyte interface in combination with an appropriated chopped light illumination in order to inhibit the effect of the electron recombination on the charge transfer kinetics (Cho et al. 2009; Gelderman et al. 2007). It requires a typical three-electrode photo-electrochemical cell (PEC) consisting of semiconductor photoanode; a cathode, made generally of Pt; and SCE as a reference electrode. The light incidence must be as a spot of controlled area.

This output photocurrent (I) signal depends on the potential V_B applied to the photoanode, and a graph as the example of Fig. 5.3 can be obtained. The magnitude of these current pulses is a function of the semiconductor surface potential S, and when $S = 0$, then current pulses disappear. Thereby, finding the dependence of the magnitude of these current peaks on the gate voltage V_B, the determination of point at which current peaks disappear is possible. This point defines directly the flat-band voltage state in semiconductor ($V_{ON} = V_{Fb}$).

Using the same three-electrode system and illumination, the photocurrent can be obtained from the transients generated under pulse visible light irradiation at a fixed bias potential. This technique was employed by Yan et al. (2011) to corroborate the

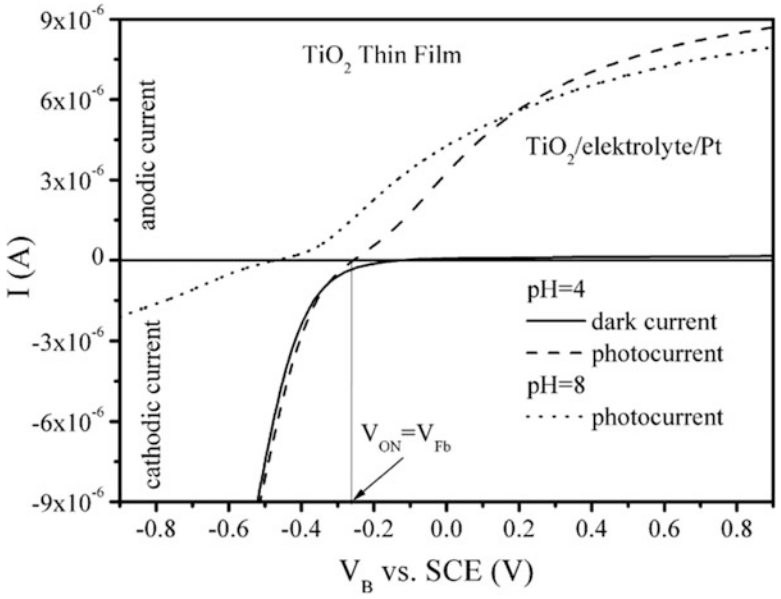

Fig. 5.3 Current–voltage I (V_B) characteristics of a TiO_2 electrode in PEC in the dark and under illumination with the white light at pH 4 and pH 8 with permission of Radecka et al. 2008

photocatalytic activity of N + S-co-doped TiO_2 nanotube arrays under visible light. They observed a constant step in photocurrent about 28 μA cm^{-2} on the photoanodes during the irradiation pulse (50s) of visible light; when light was turned off, the photocurrent returns to the initial value near zero. The results indicate that the N + S-co-doped TiO_2 nanotube arrays are sensitive to visible light and can generate a sustainable steady photocurrent under visible light irradiation.

Photocurrent intensity has been regarded as one of the most efficient methods to evaluate the photocatalytic activity of photocatalyst, and it has been recognized that a high photocurrent intensity suggests a high efficiency for electron and hole generation and separation and thus a high photocatalytic activity (Liu et al 2012).

The expected accuracy of the LPT method is typically ± 10 mV (for the most common potentiostats), while the accuracy of the V_{Fb} determination methods based on measurement of the capacitance characteristic is rarely better than ± 50 mV (Piskorski and Przewlocki 2009).

5.1.4 *Electrochemical Determination of the V_{Fb} of Particles in Suspension*

The abovementioned methods are appropriate for solid semiconductor electrodes or semiconductors deposited on a substrate (electronic conductor); however these

techniques are not appropriate when the photocatalyst is in suspension. An electrochemical method to calculate the V_{fb} for semiconductor in suspension has been proposed by Roy et al. This method is based on the measurement of the photovoltage developed under light irradiation of a suspensions containing an electron acceptor such as methyl viologen (MV^{2+};1,1′-dimethyl-4,4′-bipyridinium dichloride). This is a very simple method for determining the E_{fb} of semiconductor particles in suspension. The experimental setup requires a work electrode of Pt (1 cm^2), a reference electrode (ECS, Ag/AgCl, or another), and a combined glass electrode for pH measurements. The pH is modified by adding HNO_3 or NaOH solutions; all electrodes must be inserted through the rubber stopper, and the suspension was stirred and sparged with N_2 before and during the measurement.

In the presence of MV^{2+}, E_{fb} (e^-) will equilibrate with the Fermi level of the redox couple in solution:

$$E_f(e^-) = E_f\left(MV^{2+}/MV^{+}\right) \tag{5.5}$$

Since E_f varies with the pH of the solution and E_f (e^-) $= E_{cv} = E_{fb}$, it can be rewritten as

$$E_{fb} = E_{fb}(pH = 0) - KpH \tag{5.6}$$

For any pH value,

$$E_{fb}(pH = 0) - kpH = E^0_{\left(MV^{2+}/MV^{+}\right)} + 0.059 \log\left(MV^{2+}/MV^{+}\right) \tag{5.7}$$

Since the redox potential of the MV^{2+}/MV^{+} couple is pH independent, any change in photovoltage as a result of pH change must arise from changes in the energetics of electrons photogenerated at the particle surface, as E_{fb} shifts with respect to $E^0_{(MV2+)/(MV+)}$ with changes in solution pH:

$$0.059 \log\left(MV^{2+}/MV^{+}\right) - 0.445 = E_{fb}(pH = 0) - KpH \tag{5.8}$$

The values from the first term in Eq. (5.5) are plotted against pH to obtain E_{fb} ($pH = 0$) from the intercept, and the value of k is obtained from the slope; k represents the variation en E_{fb} per unit of pH.

5.1.5 The Band Gap Energy

Band gap energy E_g, i.e., the forbidden energy, is a very important parameter related to the electronic structure of a semiconducting material. This parameter has to match at least the energy difference 1.23 eV between the redox levels H_2O/H_2 and O_2/H_2O required for water splitting (Radecka et al. 2008). The absorption

coefficient (α) of a crystalline material depends on the photon energy according to Eq. (5.9) (Lee et al. 2001; Rajeshwar 2002):

$$\propto = A\left(hv - E_g\right)^n / hv \tag{5.9}$$

Here, A is a proportionality constant and E_g the band gap energy. For crystalline semiconductors, n depends on the electron transition type, 1/2 for direct transition and 2 for indirect transition. However, 2 has been mostly preferred to analyze the passive film (Lee et al. 2001; Miraghaei et al. 2014). The band gap energy for a passive film can be determined from an $(i_{ph}hv)^{1/2}$ versus hv plot and is estimated at the photon energy value where the i_{ph} equals 0, provided that the photocurrent (i_{ph}) for the film is proportional to the absorption coefficient: $i_{ph} = A(hv - E_g)^n/hv$.

This method was applied to obtain the E_g of the passive film zircaloy-4 (Lee et al. 2001) using a conventional three-electrode cell of 1-l multineck flask with a quartz window as a photon inlet, using the zircaloy-4 as working electrode and SCE and Pt, respectively, as reference and counter electrodes. A 300 W Xenon (Xe) arc lamp combined with a scanning digital monochromator was used to impose a monochromatic illumination (200–800 nm) to the working electrode. The band gap energy for the inner anhydrous ZrO_2 was calculated (4.30 ± 0.15 eV) by extrapolation from $(i_{ph}hv)^{1/2}$ versus hv plot.

5.1.6 Fermi Level

Another important concept in the discussion of solid-state materials is the Fermi level. The Fermi energy, E_F, of a semiconductor is defined as the energy of the topmost filled orbital at a temperature of absolute zero (Rajeshwar 2002). For an n-type semiconductor, the Fermi level lies just below the conduction band, whereas for a p-type semiconductor, it lies just above the valence band. In addition, as with metal electrodes, the Fermi level of a semiconductor electrode varies with the applied potential; for example, moving to more negative potentials will raise the Fermi level.

The semiconductor solid-state physics community has adopted the electron energy in vacuum as reference, whereas electrochemists have traditionally used the standard hydrogen electrode (SHE) scale. While estimates vary, SHE appears to lie at −4.5 eV with respect to the vacuum level. We are now in a position to relate the redox potential E_{redox} (as defined with reference to SHE) with the Fermi level E_F, redox expressed versus the vacuum reference (Rajeshwar 2002):

$$E_{F,redox} = -4.5\ \text{eV} - eE^0_{redox} \tag{5.10}$$

Subramanian et al. (2004) have determined the Fermi level and the apparent Fermi level of the TiO_2/gold nanocomposites by attaining a Nernstian equilibrium with a known C_{60}/C_{60}^- redox couple.

The experiments were carried out by mixing the known concentration of deaerated TiO_2 and Au particles first, and then irradiating the composite clusters for 30 min with UV light. A known amount of deaerated C_{60} solution was injected into the preirradiated suspension, and the equilibrium concentration of C_{60}- was determined from the absorbance at 1,075 nm.

The Fermi level (E_F) of the semiconductor is directly related to the number of accumulated electrons as illustrated in the expression

$$E_F = E_{CB} + kT \ln nc/Nc \tag{5.11}$$

E_{CB} is the conduction band energy level versus NHE, nc is the density of accumulated electrons, and Nc is the charge carrier density of the semiconductor. If we accumulate more electrons in the TiO_2 or TiO_2/Au nanoparticle system, the authors would expect a negative shift in the Fermi level of the TiO_2. By shifting the Fermi level closer to the conduction band, it would therefore be possible to improve the energetics of the semiconductor system. The apparent Fermi level (E_F*) was correlated to the concentration of the redox species by using the expression

$$E_F^* (TiO_2(e)) = E_{fb} = E^0_{Ox/Red} + 0.059 \log\left([Ox]_{eq}/[Red]_{eq}\right) \tag{5.12}$$

where E_F* is the apparent Fermi level and the flat-band potential of TiO_2 (or TiO_2/Au) and $E^\circ_{Ox/Red}$ is the standard reduction potential of the redox couple (viz., $E^\circ(C_{60}/C_{60}^-)$ −0.25 V versus NHE). By determining the equilibrium concentration of C_{60}^- in the UV-irradiated TiO_2 and TiO_2/Au suspension from the absorption at 1075 nm, the apparent Fermi level values were obtained. For the TiO_2 without gold nanoparticles was −270 mV; this represents a 270 mV more positive than the conduction band of bulk TiO_2 at neutral pH. The E_F* of the TiO_2/Au were −250, 270, and 290 using TiO_2 with gold nanoparticles of 8, 5, and 3 nm, respectively.

When the semiconductor and metal nanoparticles are in contact, the photogenerated electrons are distributed between TiO_2 and Au nanoparticles (Fermi level of Au + 0.45 V versus NHE). The transfer of electrons from the excited TiO_2 into Au continues until the two systems attain equilibration. Since the electron accumulation increases the Fermi level of Au to more negative potentials, the resultant Fermi level of the composite shifts closer to the conduction band of the semiconductor.

5.2 Characterization of Kinetic Properties in the Semiconductor–Electrolyte Interface Using Electrochemical Techniques

5.2.1 Separation of Transport, Charge Storage, and Reaction Elements in Nanostructured Oxide Semiconductor Electrodes

Electrochemical impedance spectroscopy (EIS) is an *ac* electrochemical technique very useful for characterizing, at the same time, electronic conductivity and interfacial electron transfer in nanostructured oxide electrodes permeated with electrolyte. In this sense, nanoparticulate TiO_2 films prepared on optically transparent electrodes (OTE) have been extensively studied due to their wide applications in photoelectrocatalysis.

EIS spectra are typically measured in a three-electrode cell by means of a standard potentiostat equipped with an impedance spectra analyzer. The amplitude of the *ac* signal ($|\Delta E|_{ac}$) used is about $\pm$ 10 mV, while the frequency is typically scanned between 100 kHz and 20 mHz. All the interfacial potentials must be referred against an appropriated reference electrode that controls the *dc* potential (E_{dc}) of the electrode/electrolyte interface. The counter electrodes can be Pt, Au, or W wires. The obtained spectra for films having a thickness l can be fitted to the equivalent circuit proposed by Bisquert and coworkers (Fig. 5.4) (Fabregat-Santiago et al. 2002; Terezo et al. 2001).

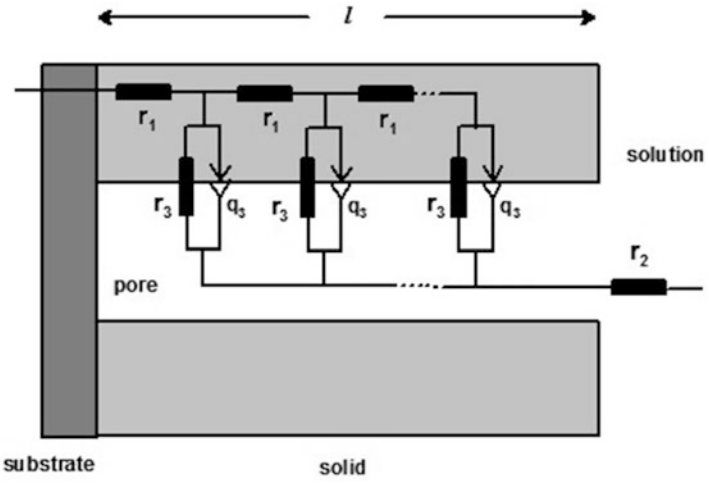

Fig. 5.4 Equivalent circuit employed to fit EIS spectra at different *dc* interfacial potentials

Electronic conductivity of the films is modeled by series resistances (r_1) representing the electron transport resistance through the electrode thickness ($R_1 = r_1 l$) and the electrolyte resistance (R_2) that separates working and reference electrodes. The electronic conductivities of the nanoporous oxide films (σ_n) are calculated from Eq. (5.13) where A and ρ represent the geometric area and porosity films, respectively:

$$\sigma_n = \frac{1}{R_1 A(1 - \rho)} \tag{5.13}$$

On the other hand, electron transfer at the oxide/electrolyte interface is modeled by constant-phase elements (CPEs, q_3) representing the charge storage into the film ($Q_3 = q_3 l$) and parallel resistances (r_3) standing for the charge transfer resistance ($R_3 = r_3/l$) which is strongly dependent from the *dc* potential.

5.2.2 *Interparticle Electron Transport Through Semiconductor Nanostructured Films*

Since the particle diameter is of the same order or smaller than the space-charge layer thickness in semiconductor thin films having high surface areas, the transportation of photoexcited electrons (e^-) and holes (h^+) through the films is controlled by diffusion (Kozuka et al. 2000; Manríquez and Godínez 2007).

This phenomenon is clearly plausible when the formation of necks between the particles takes place during the thermal sintering of the films. Figure 5.5 shows that the contact zone between *n-type* oxide nanoparticles is small, thus generating an energy barrier at this contact because of the space-charge layer as thick as or thicker than the contact diameter particle. In this way, photoexcited electrons cannot be easily transported through the oxide films, and the electrons photogenerated in the particles not bonded to the surface do not give photocurrent (j_{ph}) at the external circuit.

5.3 Determination of Photocatalytic Efficiency of Semiconductor–Electrolyte Interface Using Electrochemical Techniques

5.3.1 *Monochromatic Quantum Efficiency*

A quantum efficiency of exciton-to-charge generation is defined as the external monochromatic quantum efficiency normalized to the absorption in the active materials of the device. An upper limit of the efficiency can be determined, and

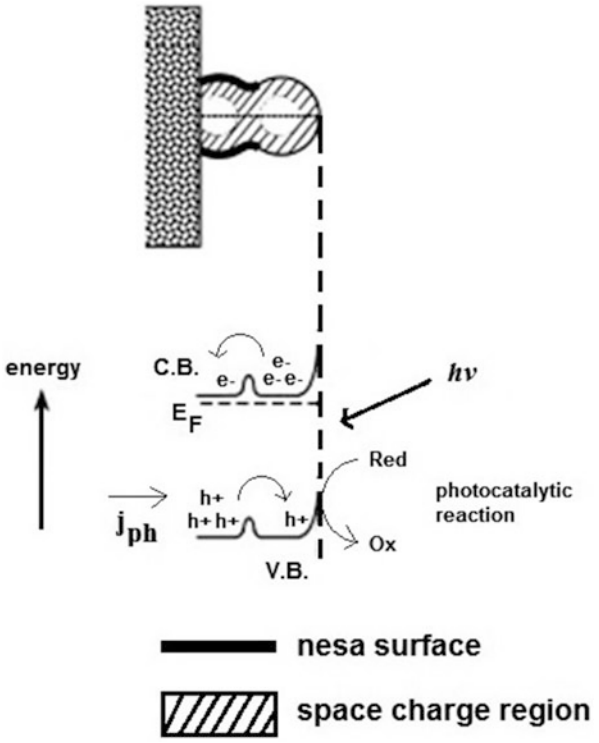

Fig. 5.5 Schematic representation of an illuminated semiconductor film containing nanometer oxide particles previously sintered, where CB and VB are the conduction and valence bands, while E_F is the Fermi level of the photogenerated electrons

results show that much of the light is absorbed in photoactive layers of the device, whereas only a fraction of the generated excitons is converted to charge carriers and can be collected as photocurrent.

Theoretical models for the action spectra of nanostructured oxide films in photoelectrochemical cells have been derived by Lindquist and coworkers (Södergren et al. 1994). These derivations where obtained by assuming that the charge carrier transport through the films is carried out by diffusion with a diffusion length constant, while recombination processes are considered to be of first order.

In this context, in Eq. (5.14) where electron flux $J_n(x,\lambda)$ is expressed as a function of electron mobility (μ_n) and density of photogenerated electrons $n(x)$, the photo-induced gradient of the electron Fermi level ($E_{F,n}$) is considered the driving force for electron transport in nanoporous photoanodes in the direction of the substrate (Vanmaekelbergh and de Jongh 1999):

$$J_n(x,\lambda) = \mu_n n(x)\left[-\frac{1}{e_0}\frac{\mathrm{d}E_{F,n}(x)}{dx}\right]_\lambda \tag{5.14}$$

According to the nature of the electron transport activation, Lindquist and coworkers reported that the electron concentration profile in nanoporous semiconductor oxide films strongly depends from the way they are illuminated (Södergren

et al. 1994). In this way, monochromatic quantum efficiencies Φ(λ) can be defined for semiconductor films illuminated through the electrolyte (EE-illumination) or through the substrate (SE-illumination) by means of Eqs. (5.15) and (5.16), respectively, which are expressed as a function of the photocurrent density (J^0), the light intensity (I_0), the minority carriers diffusion length (L), and the reciprocal absorption length (α):

$$\Phi_{SE}(\lambda) = \frac{J^0_{SE}}{e_0 I_0} = \frac{\left[-L\alpha_\lambda \cos h(l/L) + \operatorname{sen} h(l/L) + L\alpha_\lambda e^{-\alpha_\lambda l}\right] L\alpha}{\left(1 - L^2\alpha_\lambda^2\right)\cos h(l/L)} \tag{5.15}$$

$$\Phi_{EE}(\lambda) = \frac{J^0_{EE}}{e_0 I_0} = \frac{\left[L\alpha_\lambda \cos h(l/L) + \operatorname{sen} h(l/L) - L\alpha_\lambda e^{\alpha_\lambda l}\right] L\alpha_\lambda e^{-\alpha_\lambda l}}{\left(1 - L^2\alpha^2\right)\cos h(l/L)} \tag{5.16}$$

5.3.2 Photochemical Thermodynamic Efficiency Factor (PTEF)

The photochemical thermodynamic efficiency factor (PTEF) is an energy ratio equating the energy used to achieve the photocatalytic conversion of organic molecules over the energy absorbed by the photocatalyst and evaluates the performance of photocatalytic reactors on a thermodynamic basis (Serrano and De Lasa 1997), with the equation of the reactor's efficiency:

$$\text{PTEF} = \eta = \frac{Q_{\text{used}}}{Q_a} \tag{5.17}$$

Q_a represents the irradiation energy absorbed and Q_{used} the irradiation energy used for the desired formation of $^{\bullet}$OH radicals which then interact with adsorbed species. The PTEF is a generally applicable parameter as it is not restricted to either a homogeneous or a heterogeneous photoconversion chemical process.

More specifically, the Q_{used} in the photoconversion process can be represented via the $r_{\bullet OH}\Delta H_{\bullet OH}W_{irr}$ group with the PTEF being represented by

$$\text{PTEF} = \eta = \frac{r_{\bullet OH}\Delta H_{\bullet OH}W_{irr}}{Q_a} \tag{5.18}$$

where $r_{\bullet OH}$ represents the rate of formation of $^{\bullet}$OH radical groups per unit weight of irradiated catalyst, $\Delta H_{\bullet OH}$ is the enthalpy of formation of an $^{\bullet}$OH group, and W_{irr} is the total amount of irradiated catalyst. Alternatively, a PTEF definition can be introduced based on A_{irr}, the area of irradiated catalyst,

$$\text{PTEF} = \eta = \frac{r'_{\bullet OH}\Delta H_{\bullet OH}W_{irr}}{Q_a} \tag{5.19}$$

While photocatalytic reactions are frequently considered to be pseudo-homogeneous reactions with a rate based on either the unit volume of irradiated catalyst or the total reactor volume, definitions of the PTEF can be given as follows:

$$\mathrm{PTEF} = \eta = \frac{r''_{\bullet\mathrm{OH}} \Delta H_{\bullet\mathrm{OH}} W_{\mathrm{irr}}}{Q_a} \tag{5.20}$$

$$\mathrm{PTEF} = \eta = \frac{r'''_{\bullet\mathrm{OH}} \Delta H_{\bullet\mathrm{OH}} W_{\mathrm{irr}}}{Q_a} \tag{5.21}$$

where $r_{\bullet\mathrm{OH}} W_{\mathrm{irr}} = r'_{\bullet\mathrm{OH}} A_{\mathrm{irr}} = r''_{\bullet\mathrm{OH}} V_{\mathrm{irr}} = r'''_{\bullet\mathrm{OH}} V$, with the rate of formation of $^{\bullet}$OH radicals and the enthalpies of $^{\bullet}$OH radical formation. Regarding the rate of $^{\bullet}$OH radical formation, it can be considered to be the sum of two terms, the rate of $^{\bullet}$OH consumption and the rate of $^{\bullet}$OH accumulation with $r_{\bullet\mathrm{OH,c}}$ having a negative sign (consumption of $^{\bullet}$OH radicals):

$$r_{\bullet\mathrm{OH}} = -r_{\bullet\mathrm{OH,c}} + r_{\bullet\mathrm{OH,acc}} \tag{5.22}$$

Evaluation of $^{\bullet}$OH radical ($r_{\bullet\mathrm{OH}}$) formation presents inherent problems. The $^{\bullet}$OH radicals react with both the adsorbed model pollutant and the adsorbed intermediates (Pelizzetti et al. 1992; Turchi and Ollis 1990). Furthermore, the evaluation of the rate of $^{\bullet}$OH radicals involves stoichiometric coefficients such as

$$r_{\bullet\mathrm{OH,c}} = \nu \sum_{\mathrm{P}} \frac{r_{\mathrm{P}}}{\nu_{\mathrm{P}}} \tag{5.23}$$

The stoichiometric coefficient for the consumption of $^{\bullet}$OH groups is ν, and r_{p} and ν_{p} the rate and the stoichiometric number for the consumption of organic chemical species (including model pollutant and intermediate species) respectively. As a result, $r_{\bullet\mathrm{OH}}$ can be expressed as follows:

$$r_{\bullet\mathrm{OH}} = -\nu \sum_{\mathrm{P}} \frac{r_{\mathrm{P}}}{\nu_{\mathrm{P}}} + r_{\bullet\mathrm{OH,acc}} \tag{5.24}$$

At the beginning of the photoconversion, when the surface concentration of all chemical species is equal to the surface concentration of the model compound, the model compound is the only $^{\bullet}$OH group scavenger. Therefore

$$\sum_{\mathrm{P}} \frac{r_{\mathrm{P}}}{\nu_{\mathrm{P}}} = \frac{\nu r_{1,\mathrm{in}}}{\nu_1} \tag{5.25}$$

with $r_{1,\mathrm{in}}$ representing the rate of consumption of the model pollutant and ν_1 the stoichiometric coefficient for the consumption of the model pollutant. Alternatively,

$$r_{\bullet OH} = -\frac{\nu r_{1,in}}{\nu_1} + r_{\bullet OH,acc} \tag{5.26}$$

At initial conditions, the model pollutant concentration is very high, in large excess with respect to the other species, and it is very likely that the model pollutant is going to consume all the $^{\bullet}OH$ radicals with no accumulation of the OH groups ($r_{\bullet OH,acc} = 0$). As a result, the following is achieved:

$$r_{\bullet OH} = -\frac{\nu r_{1,in}}{\nu_1} \tag{5.27}$$

Under the situation described, the PTEF can be evaluated as

$$PTEF = \eta = \frac{-\frac{\nu}{\nu_1} r_{1,in} \Delta H_{\bullet OH} W_{irr}}{Q_a} \tag{5.28}$$

Or alternatively,

$$PTEF = \eta = \frac{-\frac{\nu}{\nu_1} r'_{1,in} \Delta H_{\bullet OH} W_{irr}}{Q_a} \tag{5.29}$$

$$PTEF = \eta = \frac{-\frac{\nu}{\nu_1} r''_{1,in} \Delta H_{\bullet OH} W_{irr}}{Q_a} \tag{5.30}$$

$$PTEF = \eta = \frac{-\frac{\nu}{\nu_1} r'''_{1,in} \Delta H_{\bullet OH} W_{irr}}{Q_a} \tag{5.31}$$

Frequently, it is observed that photocatalytic reactions follow the Langmuir–Hinshelwood model

$$r_{1,in} = \frac{-k_1 C_1}{1 + K_1 C_1} \tag{5.32}$$

with k_1 representing the apparent intrinsic constant for the pollutant photoconversion, C_1 the model pollutant volumetric concentration, and K_1 the model pollutant adsorption constant. At large pollutant concentrations, $1 << K_1 C_1$ can be expected, and consequently the rate of photoconversion of a model pollutant shows a maximum value. Under these conditions, the PTEF reaches as well an upper limit:

$$PTEF_{max} = \eta_{max} = \frac{-\frac{\nu}{\nu_1} (r_{1,in})_{max} \Delta H_{\bullet OH} W_{irr}}{Q_a} \geq \eta \tag{5.33}$$

Or

$$\mathrm{PTEF}_{\max} = \eta_{\max} = \frac{-\frac{\nu}{\nu_1}\left(r'_{1,\mathrm{in}}\right)_{\max}\Delta H_{\bullet\mathrm{OH}}W_{\mathrm{irr}}}{Q_a} \geq \eta \tag{5.34}$$

$$\mathrm{PTEF}_{\max} = \eta_{\max} = \frac{-\frac{\nu}{\nu_1}\left(r''_{1,\mathrm{in}}\right)_{\max}\Delta H_{\bullet\mathrm{OH}}W_{\mathrm{irr}}}{Q_a} \geq \eta \tag{5.35}$$

$$\mathrm{PTEF}_{\max} = \eta_{\max} = \frac{-\frac{\nu}{\nu_1}\left(r'''_{1,\mathrm{in}}\right)_{\max}\Delta H_{\bullet\mathrm{OH}}W_{\mathrm{irr}}}{Q_a} \geq \eta \tag{5.36}$$

To calculate the $\mathrm{PTEF}_{\max}$ value for a specific photocatalytic system, the initial concentration of the model pollutant has to be increased progressively until the PTEF approaches a constant value, the $\mathrm{PTEF}_{\max}$ (Serrano and De Lasa 1997):

$$\mathrm{PTEF}_{\max} = \eta_{\max} \geq \mathrm{PTEF} = \eta \tag{5.37}$$

This upper value for the PTEF is an intrinsic characteristic of a photocatalytic reactor as well as of the pollutant being photoconverted. This efficiency factor includes various reactor characteristics such as the absorbed irradiation, the rate of photoconversion, and the enthalpy of $^{\bullet}$OH group formation. A relationship can also be established between the quantum yield and the PTEF given that the $\mathrm{PTEF}_{\max}$ can be expressed as

$$\mathrm{PTEF}_{\max} = \eta_{\max} = \frac{-\frac{\nu}{\nu_1}\left(r_{1,\mathrm{in}}\right)_{\max}W_{\mathrm{irr}}\alpha\left[\frac{N_A hc}{\lambda}\right]}{Q_a}\frac{\Delta H_{\mathrm{OH}}}{\alpha\left[\frac{N_A hc}{\lambda}\right]} \tag{5.38}$$

with α being the number of photon needed for the formation of a $^{\bullet}$OH group, N_{A} the Avogadro number (6.023×10^{23} molecules mol^{-1}), h the Planck constant (6.62×10^{34} Js photon^{-1}), c the speed of light in vacuum (2.997×10^{10} cm s^{-1}), and λ the average wave length (nm). Then,

$$\mathrm{PTEF}_{\max} = \eta_{\max} = \varphi_{\mathrm{in,max}}\eta_{\bullet\mathrm{OH}} \tag{5.39}$$

with $\varphi_{\mathrm{in,max}}$ representing the maximum quantum yield (defined at initial conditions), or the maximum fraction of photons absorbed in the photocatalyst that results in the formation of $^{\bullet}$OH radicals, and $\eta_{\bullet\mathrm{OH}}$ being the fraction of the photon energy used in the formation of $^{\bullet}$OH radicals. The last equation shows that energy efficiency evaluations using PTEF require not only a maximum quantum yield definition at initial conditions, based on the energy absorbed by the catalyst, but also $\eta_{\bullet\mathrm{OH}}$, the fraction of the photon energy used in forming $^{\bullet}$OH groups. The product of these two parameters provides an assessment of the energy efficiency of a photocatalytic reactor system.

The PTEF is a dimensionless quantity, as required by thermodynamic consistency. The PTEF definition can be broadly applied, covering various kinetic models and being appropriate for various photochemical reactors, either homogeneous (in solution) or heterogeneous (in interface). In practice, the calculation of $PTEF_{max}$ can be done using the corresponding equations for conditions where the initial photoconversion rates reach maximum values and with $\nu/\nu_1 = 1$ (De Lasa et al. 2005).

5.3.3 Relative Photonic Efficiency (ξ_r)

Photon efficiency (ξ) is used to facilitate the comparison of the efficacy of reactor designs (which differed in size and hence the residence time), as

$$\xi = \frac{C_o V}{I_o} \tag{5.40}$$

where C_o is the initial concentration, V is the volume flow rate, and I_o is the light intensity. In the case of relative photonic efficiency, a specific wavelength (ξ_r) is in order (Rajeshwar and Ibañez 1997).

5.3.4 Quantum Yield (Φ)

The experimental determination of the photocatalytic activity of heterogeneous systems has been an important topic in the proper characterization of different materials with catalytic photoactivity. Even with the commonly accepted view that the quantum yield (Φ) of a heterogeneous photochemical reaction is an important parameter in characterizing the activity of photocatalyst material, its practical application is seldom achieved. A major reason for this situation is the lack of a simple reliable experimental method to determine the quantum yield in any photocatalytic laboratory. According to the pioneer investigations carried out by Emeline et al. (2006) and Brandi et al. (2003), an interesting simple method for the direct experimental determination of quantum yields of photoreactions in liquid–solid heterogeneous systems with dispersed solid nano or microparticles based on the application of the concept of the black body-like reactor has been proposed.

The quantum yield of a heterogeneous photochemical reaction is defined exactly in accordance with the definition of the quantum yield in general homogeneous photochemistry, i.e., the number of molecules of a given reactant consumed or of a given product formed per photon of light absorbed by the photocatalyst at a given wavelength Eq. (5.41):

$$\Phi = \frac{N_{\mathrm{m}}}{N_{hv}} \tag{5.41}$$

This definition can also be used (Emeline et al. 2006; Brandi et al. 2003) for heterogeneous photocatalytic processes when the system has reached the stationary state. As recommended by Emeline and Serpone (2002) and by Serpone and Salinaro (1999), for consistency, both quantities must be evaluated under otherwise identical conditions and preferably at the same time. In practice, the quantum yield is typically given in terms of "rates." For instance, the numerator represents the rate of reaction, and the denominator represents the rate of absorption of photons Eq. (5.42):

$$\Phi = \frac{N_{\mathrm{m}}/\mathrm{d}t}{N_{hv}/\mathrm{d}t} \tag{5.42}$$

This equation should also be used for heterogeneous photoreactions whether the photocatalyst nature of material has been tested. In such cases, initial reaction rates are typically used to characterize the reproducible initial state of the photocatalyst material. The major experimental obstacle in measuring quantum yields of heterogeneous photoreactions is how to estimate the number of photons actually absorbed by the solid photocatalyst.

In this context, Eq. (5.43) denotes the balance between the fractions of reflected (R), transmitted (T), and absorbed (A) light in the system following the conservation law. Subsequently, determination of the fraction of absorbed light requires understanding of the fractions of reflected and transmitted light, a feat that cannot be achieved by application of traditionalist spectroscopic methods because of the diffuse scattering of light in dispersed photocatalytic systems. More sophisticated determinations are required. This has produced many works to report a so-called quantum yield evaluated on the basis of the incident light rather than the light actually absorbed by the heterogeneous system (Emeline et al. 2000):

$$A + R + T = 1 \tag{5.43}$$

Sun and Bolton (1996) and Serpone and Salinaro (1999) also suggested the application of an integrating sphere to estimate the fraction of absorbed light and established a standard protocol to approximate the quantum yield of any heterogeneous photoreaction using the photodegradation of phenol over TiO_2 (Degussa P25) as a typical photoreaction based on the concept of a relative photonic efficiency (ξ_{r}; Eq. 5.44) (Panida et al. 2009; Critchley et al. 2006; Cheadle et al. 2001):

$$\Phi = \xi_{\mathrm{r}}\Phi_{\mathrm{st}} \tag{5.44}$$

where Φ denotes the quantum yield of the photochemical process being examined and Φ_{st} is the quantum yield of the standard heterogeneous photochemical reaction. The application of this standard protocol should significantly simplify the

procedure for determining the quantum yield of any photoreaction in liquid–solid heterogeneous systems, since with the known quantum yield of the standard reaction (used as a secondary actinometer), the experimental task of measuring the reaction rate of the photoreaction over the same photocatalyst is thereby simplified. The relative photonic efficiency is simply the ratio of the reaction rate of the photoreaction under examination to the standard photoreaction Eq. (5.45):

$$\xi_r = \frac{\Phi}{\Phi_{st}} = \frac{dN/dt}{dN_{st}/dt} \tag{5.45}$$

Even with this simplicity, however, the proposed protocol does not find significant wide application in the photocatalytic community, with researchers continuing to report the so-called apparent quantum yields based on the photon flow of the incident light that has been termed "photonic efficiency." In the early 1970s, Basov and Solonitsyn (1973) proposed the concept of the black body reactor to estimate the (Φ) photoreaction in gas–solid heterogeneous systems.

Since then, this method was positively used to estimate the spectral dependences of the quantum yields of the photostimulated adsorption of oxygen, hydrogen, and methane on ZnO and TiO_2 semiconductors as well as on other metal oxides (Emeline et al. 2000; Basov et al. 1977; Cherkashin et al. 1980; Emeline et al. 1997).

A.V. Emeline et al. in 2006 measured the quantum yield in liquid–solid heterogeneous system for the phenol photodegradation over *n*-doped TiO_2 using a reactor based in the concept of the black body. Figure 5.6 shows an image of the modified reactor. The system involves a beaker containing the liquid phase with a dispersed photocatalyst and a cavity with a quartz wall located in the center of the beaker. The solution is mechanically stirred to avoid mass transfer limitation problems. The optical fiber (diameter, 2 mm) is inserted into the cavity to direct the light inside the cavity. Ever since the area of the fiber cross section is much smaller than the total area of the cavity wall; for this the authors take on that back reflection is negligible and that all the light (including the diffuse reflected light) is eventually directed inside the solution. Thus, in this reactor, the reflected light will always be negligible; that is, $R \to 0$. A very high optical density of the heterogeneous system can always be achieved so that $T \to 0$ by increasing the loading of the photocatalyst at a sufficient distance between the wall of the inner cavity and the wall of the beaker (2.5 cm, Emeline et al. 2006; Brandi et al. 2003).

Figure 5.7 shows a decay of the transmittance measured with the UV–Vis spectrometer and integrating sphere assembly with increasing light path length in a solution containing TiO_2 (Degussa P25) at a photocatalyst concentration of 1 g/L. As manifest from the data, the loss of transmittance of light for a 1 cm path length does not exceed 1 % in the spectral region of the fundamental absorption of the photocatalyst. In light of this result, the authors understand that all the light directed inside the cavity is eventually absorbed in the system. Thus, to measure the quantum yield of a heterogeneous photoreaction, one needs to know only the light irradiance at the outlet of the optical fiber and the rate of the heterogeneous

Fig. 5.6 Photography of the black body reactor for measurement of the quantum yield in liquid–solid heterogeneous system. From Emeline et al. 2006. Copyright 2006 American Chemical Society

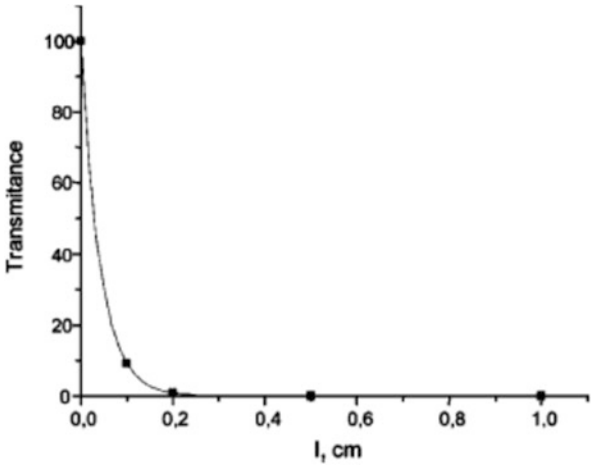

Fig. 5.7 Dependence of the transmittance ($\lambda = 365$ nm) of the solution containing TiO_2 (Degussa P25; photocatalyst loading 1 g/L) measured with an integrating sphere on the light path length

photochemical reaction determined by any conventional method (Emeline et al. 2006; Brandi et al. 2003).

With this device Emeline et al. (2006) and Brandi et al. (2003) tested the quantum yield of phenol photodegradation over N-doped TiO_2 as an early application of this method. The authors selected to measure the quantum yield of the photodegradation of organic molecule over semiconductor at two different wavelengths, 365 nm which corresponds to the fundamental absorption of TiO_2 and 436 nm corresponding to the N-doping-induced visible absorption band. In this assay the authors report the dependence of the transmittance of the heterogeneous

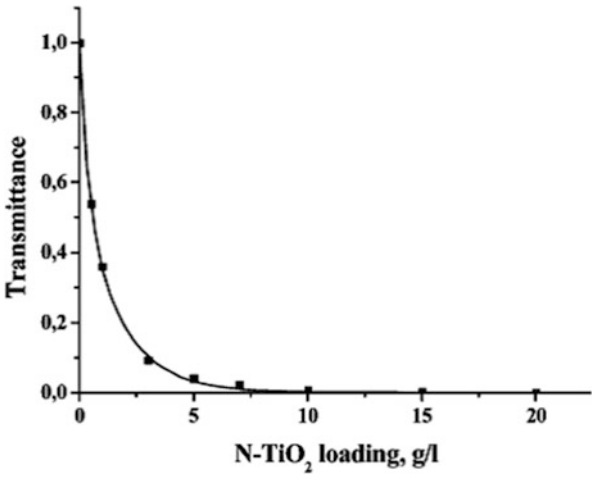

Fig. 5.8 Decay of transmittance measured with the integrating sphere with increase of the photocatalyst loading at 436 nm (light path length, 1 cm) (Emeline et al. 2006)

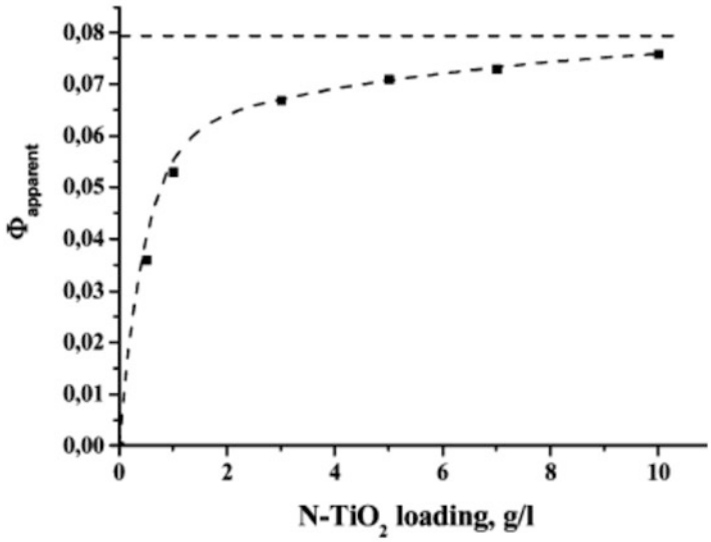

Fig. 5.9 Increase of the apparent quantum yield with increase in the photocatalyst loading (Emeline et al. 2006)

system measured with the integrating sphere assembly on photocatalyst loading at 436 nm (Fig. 5.8).

These results indicate that loss of transmittance of light for a 1 cm path length and photocatalyst loading greater than 7 g/L does not exceed 5 %, which means that most of the light does not pass outside the reactor setup. Also they measured the dependence of the apparent quantum yield on photocatalyst loading calculated with respect to the irradiance of the actinic light impinging on the reactor (Fig. 5.9).

In the light of these results, the authors used the term apparent quantum yield, instead of the otherwise more appropriate term photonic efficiency, to emphasize that regardless of the photocatalyst loading. For that reason, the system tested can also be applied to measure quantum yields in a spectral range corresponding to the extrinsic absorption caused by impurities or defects, provided that one uses a sufficiently high photocatalyst loading to satisfy the condition $T \to 0$. Under such conditions, then, the quantum yield for the photodegradation of phenol in N-doped TiO_2 aqueous dispersions under irradiation at 365 nm (intrinsic absorption of TiO_2) is $\Phi = 0.12$, whereas under irradiation in the extrinsic absorption at 436 nm induced by the N-doping Φ is 0.08 (Emeline et al. 2006; Brandi et al. 2003).

On the other hand, Thornton and Raftery in (2012) proposed the evaluation of quantum efficiency of the undoped and carbon-doped cadmium indate ($CdIn_2O_4$) powders which were prepared using a sol – gel pyrolysis method, as a function of hydrogen generation. The quantum efficiency of the optimized Pt-loaded C-doped $CdIn_2O_4$ was measured as a function of wavelength using a series of band-pass filters and irradiating an excess mass of sample ($\sim$1.0 g). The apparent quantum efficiency (Φ) was calculated using the following Eq. (5.46):

$$\mathrm{F}(\%) = (\text{no. of } \mathrm{H_2}\text{molecules} \times 2/\text{no. of incident photons}) \times 100\% \qquad (5.46)$$

The number of incident photons was calculated using theme-assured power output of the lamp through each filter.

In another work, Corboz and coworkers (2000) evaluated a framework to determine the quantum efficiency η of a photoreaction in a porous layer of a photocatalyst material. This model incorporates a position-dependent source term mirroring the light intensity profile in the layer and an effective diffusion coefficient D_{eff}. It allows for a simultaneous determination of η as well as of D_{eff}. The method is applied to the photosynthesis of CH_4 from gaseous H_2O and CO_2 at the solid/gas interface of a porous layer of TiO_2 (Degussa P25).

In this research the authors describe the quantum efficiency η of the reaction as the number of product molecules divided by the total number of photons absorbed. Because of a subtle interplay between the optical penetration depth and the diffusion length of the free carriers generated, the quantum efficiency of a photochemical reaction at a semiconductor surface can even become wavelength dependent (Yu et al. 2003; Zhang and Yu 2003).

An interesting modeling of diffusion inside a porous photocatalyst was proposed where the modeling of the material flows in the porous layer is much simplified by the fact that only the flow of products must be considered. Because of the very small quantum efficiency of the reaction under consideration, the reactants in the layer are not so severely depleted during the irradiation time of 600 s that their surface coverage on the photocatalyst is expected to be altered significantly. We further assume that the product flux is proportional to the concentration gradient in accordance with the equation

$$j(x) = -D_{\text{eff}} \frac{\partial}{\partial x} c(x,t) \tag{5.47}$$

The microscopic processes involved will not be specified, and the effective diffusion coefficient D_{eff} is a phenomenological parameter determined by measurement. Mass conservation yields the diffusion equation (5.48):

$$\frac{\partial}{\partial t} C(x,t) = D_{\text{eff}} \frac{\partial^2}{\partial^2 x} C(x,t) + q(x) \tag{5.48}$$

where the source term $q(x)$ is given by Eq. (5.49):

$$q(x) = \eta K E(x) \tag{5.49}$$

Equation (5.49) implies that η is constant and independent of the light intensity E, which is not necessarily the case. Equation (5.49) states furthermore that the source strength does not depend on the concentration of the reactant, that is, that the effect of reactant consumption can be neglected.

Wang et al. in 2004 investigated the photocatalytic activity of the samples (0.1 g/l) by measuring the quantum yield, Φ_{HCHO}, of HCHO formed from aqueous methanol at pH 3.5 under different conditions. In CW photolysis of the oxygenated suspensions (300–400-nm UV light, 8×10^{-7} Einstein L^{-1} s^{-1} photon absorption rate), the platinized photocatalysts (1 wt % Pt) enhance Φ_{HCHO} by a factor of 1.5–1.7 with respect to neat colloidal TiO_2 where Φ_{HCHO} is 0.02.

Previously, Sun and Bolton (1996) studied the photocatalytic formation of formaldehyde (HCHO) from methanol in oxygenated aqueous suspensions of TiO_2 (anatase) particles and derived the quantum yield of the OH radical considered as the oxidizing intermediate (Martínez et al. 2013). Based on this knowledge authors carried out the same oxidation reaction in order to investigate the activity of different types of titanium dioxide photocatalysts (colloidal TiO_2 particles of nominally 2.4 nm diameter, Degussa P25, Sachtleben Hombikat UV 100) by the measurement of the HCHO quantum yield, Φ_{HCHO}, after continuous UV photolysis of their aqueous suspensions containing methanol (Neppolian et al. 2002; Anpo and Takeuchi 2003).

In this study the activity of the photocatalysts under different conditions of photolysis was assessed by the determination of the quantum yield, Φ, of HCHO formation by photooxidation of methanol, whereΦ is defined as

$$\Phi = R/I_{\text{a}} \tag{5.50}$$

and

$$I_{\text{a}} = I_0 F_{\text{s}} \tag{5.51}$$

R is defined as the photochemical formation rate of HCHO. I_a and I_0 are the absorbed and incident photon fluxes, respectively, in units of inset in L^{-1} s^{-1}. In CW photolysis, F_s is the integrated absorption fraction of the sample over the wavelength range used:

$$F_S = \frac{\int_{\lambda_1}^{\lambda_2} I_\lambda T_\lambda^f \mathrm{d}\lambda}{\int_{\lambda_1}^{\lambda_2} I_\lambda T_\lambda^f \mathrm{d}\lambda} \tag{5.52}$$

I_λ is the relative incident photon flux in the wavelength band dλ, T_λ^f is the transmittance of the filter used in the experiment, and

$$f_\lambda^S = 1 - T_\lambda^S = 1 - 10 - A_\lambda^S \tag{5.53}$$

$f_\lambda{}^S$ is the fraction of light absorbed at wavelength λ. $T_\lambda{}^s$ and $A_\lambda{}^s$ are the transmittance and absorbance, respectively, of the sample at wavelength λ. I_0 and Fs were determined by chemical actinometry (Wang et al. 1992) and spectrophotometry. In monochromatic laser photolysis, Fs is identical with $f_\lambda{}^s$ (Eq. 5.53).

Each material was tested to evaluate the photocatalytic activity by the measurement of the quantum yield, Φ_{HCHO}, of HCHO formed by photocatalytic oxidation of methanol. Upon exposure of O_2-saturated aqueous suspensions, containing one of the photocatalysts and methanol, to 300–400 nm, HCHO was produced and identified quantitatively by HPLC analysis.

Evidently, platinization has a strong promoting effect on the formation of HCHO in TiO_2-based photocatalysis. HCHO increases by up to 50–70 % when compared with that value on neat TiO_2 particles. From Fig. 5.10 it is also seen that photochemical platinization of the TiO_2 particles yields a more efficient photocatalyst (PtTi-S1) than mixing of the colloidal components of Pt and TiO_2 (PtTi-S2).

For this case, the authors proposed the internal quantum yield (Φ_{Int}) estimation by means of the observed absorption of the film and the value of Φ_{Ext} at each wavelength, by use of $\Phi_{Int} = \Phi_{Ext}/(1-R)$, where R is the measured reflectance. For the porous electrode, Φ_{Int} was constant at a value of ~0.5 for $\lambda < 420$ nm, while the measured absorbance approached zero for $\lambda > 420$, yielding unreliable values for Φ_{Int}. In contrast, for the compact electrode, Φ_{Int} rose slowly as the illumination wavelength was decreased and only reached ~0.4 at $\lambda = 280$ nm. The porous electrode thus produced a sixfold increase in Φ_{Int} at $\lambda = 350$ nm relative to the compact film.

In the light of these sentences, internal quantum yields for porous WO_3 electrodes were proposed for use in light-driven water-splitting devices as a photoanode (Hodes et al. 1976; Tacca et al. 2012). WO_3 absorbs more of the solar spectrum than most other wide band gap metal oxides and is stable in acidic medium. WO_3 clearly does not have an optimal band gap for solar energy conversion applications, but is a useful model system to test the hypothesis of concern in this work. As shown in

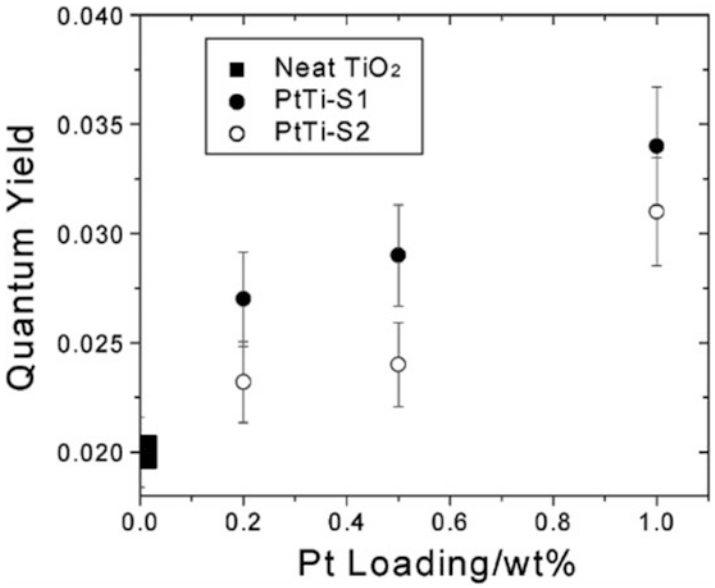

Fig. 5.10 Quantum yields of photocatalytic formaldehyde formation from methanol in the presence of PtTi-S1 and PtTi-S2 as a function of Pt loading. For comparison: neat colloidal TiO_2 (F_s) 0.24 derived from Eq. (5.13) in the wavelength range of 300–400 nm (Wang et al. 2004)

Fig. 5.10, the onset of the spectral response of both the compact and porous WO_3 electrodes occurred at $\lambda \sim 460$ nm, in agreement with the 2.6 eV band gap of WO_3 (Butler et al. 1976; Miller et al. 2006).

Although the onset of the spectral response Φ_{Ext} was principally determined by the band gap, the efficiency with which incident photons can be converted to current was dependent on the structure of the film. Even though the porous films absorbed only about half as much of the incoming light as the compact film, for $\lambda > 300$ nm, the Φ_{Ext} values of the porous WO_3 films were higher than those of the compact WO_3 films (Fig. 5.11a). Furthermore, at all wavelengths, the Φ_{Int} values of porous WO_3 films were much higher than those of the compact films (Fig. 5.11b). Notably, Φ_{Int} was not corrected for the actual optical reflection losses of the porous film, suggesting that Φ_{Int} for the porous film was higher than reported in Fig. 5.11b.

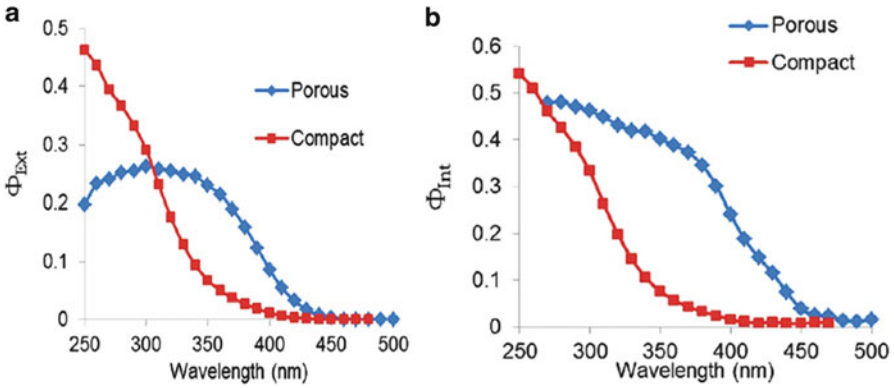

Fig. 5.11 Plot of the wavelength dependence of (**a**) the external quantum yield and (**b**) the internal quantum yield at the formal potential for water oxidation for compact (*red square*) and porous (*blue rhombohedral*) WO_3 electrodes in contact with 0.10 M HCl (aq) (pH = 1.0) (Reyes-Gil et al. 2013)

Concluding Remarks

The photoelectrochemical technique has been found to have an advantage of unique site-selective dissolution and to contribute not only to micro-tailoring of semiconductor surface but also to further characterization of grain structure and established aspects related to the semiconductor energy band model and the electrostatics at semiconductor–electrolyte interfaces in the dark, processes of light absorption, electron–hole generation, and charge separation at these interfaces. In general, the electrochemical techniques are very useful to characterize photocatalytic materials in a short time and specific thermodynamic and kinetic parameters to understand the determination of photocatalytic efficiency of semiconductor materials.

References

Anpo M, Takeuchi M (2003) The design and development of highly reactive titanium oxide photocatalysts operating under visible light irradiation. J Catal 216:505–516

Bard AJ, Faulkner LR (2000) Electrochemical methods: fundamentals and applications, 2nd edn. John Wiley& Sons, New York, p 850. ISBN ISBN: 0-471-04372-9

Bard AJ, Faulkner LR (2001) Electrochemical methods: fundamentals and applications, vol 6, 2nd edn. John Wiley & Sons, New York, pp 11–13

Basov LL, Solonitzyn YP. Patent No. 387730. Bull. InVention Committee USSR 1973, No. 28

Basov LL, Kuzmin GN, Prudnikov IM, Solonitzyn YP (1977) In: Uspekhi Fotoniki, Vilesov ThI (eds) Advances in Photonics, Leningrad State University, 6, p 82

Beranek R (2011) (Photo)electrochemical methods for the determination of the band edge positions of TiO_2-based nanomaterials. Adv Phys Chem 2011:1–20. doi:10.1155/2011/786759

Brandi RJ, Citroni MA, Alfano OM, Cassano AE (2003) Absolute quantum yields in photocatalytic slurry reactors. Chem Eng Sci 58(3–6):979–985

Butler MA, Nasby RD, Quinn RK (1976) Tungsten trioxide as an electrode for photoelectrolysis of water. Solid State Commun 19:1011–1014

Cheadle EM, Batchelder DN, Evans SD, Zhang HL, Fukushima H, Miyashita S, Graupe M, Puck A, Shmakova OE, Colorado R, Lee TR (2001) Polymerization of semi-fluorinated alkane thiol self-assembled monolayers containing diacetylene units. Langmuir 17:6616–6621

Cho IS, Kwak C, Kim DW, Lee S, Hong KS (2009) Photophysical, photoelectrochemical, and photocatalytic properties of novel $SnWO_4$ oxide semiconductors with narrow band gaps. J Phys Chem C 113(24):10647–10653

Corboz M, Alxneit I, Stoll G, Rudolf H (2000) On the determination of quantum efficiencies in heterogeneous photocatalysis. J Phys Chem B 104:10569–10577

Critchley K, Zhang LX, Fukushima H, Ishida M, Shimoda T, Bushby RJ, Evans SD (2006) Soft-UV photolithography using self-assembled monolayers. J Phys Chem B 110:17167–17174

De Lasa H, Serrano B, Salaices M (2005) Photocatalytic reaction engineering. Ed. Springer, USA, ISBN 978-0-387-27591-8

Emeline AV, Serpone N (2002) Suggested terms and definitions in photocatalysis and radiocatalysis. Int J Photoenergy 4:91–131

Emeline AV, Kuzmin GN, Purevdorj D, Shenderovich IG (1997) Spectral and temperature dependencies of simple molecules photoadsorption quantum yields for dispersed zinc oxide. Russian J Kinet Katal 38:446–450

Emeline AV, Kuzmin GN, Purevdorj D, Ryabchuk VK, Serpone N (2000) Spectral dependencies of the quantum yield of photochemical processes on the surface of wide band gap solids. 3. Gas/solid systems. J Phys Chem B 104:2989–2999

Emeline AV, Zhang X, Jin M, Murakami T, Fujishima A (2006) Application of the "black body like" reactor for the measurements of the quantum yield of photochemical reactions in heterogeneous systems. J Phys Chem B 110:7409–7413

Fabregat-Santiago F, Garcia-Belmonte G, Bisquert J, Zaban A, Salvador P (2002) Decoupling of transport, charge storage, and interfacial charge transfer in the nanocrystalline TiO_2/electrolyte system by impedance methods. J Phys Chem B 106:334–339

Gelderman K, Lee L, Donne SW (2007) Flat-band potential of a semiconductor: using the Mott–Schottky equation. J Chem Educ 84(4):685

Hodes G, Cahen D, Manassen J (1976) Tungsten trioxide as a photoanode for a photoelectrochemical cell (PEC). Nature 260:312–313

Hodes G, Manassen J, Cahen D (1981) Effect of surface etching and morphology on the stability of CdSe/Sx = photoelectrochemical cells. J Electrochem Soc 128:2325–2330

Jacobsson TJ, Edvinsson T (2012) Photoelectrochemical determination of the absolute band edge positions as a function of particle size for ZnO quantum dots. J Phys Chem C 116(29):15692–15701

Kozuka H, Takahashi Y, Zhao G, Yoko T (2000) Preparation and photoelectrochemical properties of porous thin films composed of submicron TiO_2 particles. Thin Solid Films 358:172–179

Kuhn-Kuhnenfeld F (1972) Selective photoetching of gallium arsenide. J Electrochem Soc 119:1063–1068

Lee S, Cho E, Ahn S, Kwon H (2001) Photo-electrochemical analysis of the passive film on zircaloy-4-. Electrochim Acta 46(17):2605–2611

Liu Y, Xie C, Li J, Zou T, Zeng D (2012) New insights into the relationship between photocatalytic activity and photocurrent of TiO_2/WO_3 nanocomposite. Appl Catal A 433–434:81–87

Manríquez J, Godínez LA (2007) Tuning the structural, electrical and optical properties of Ti(III)-doped nanocrystalline TiO_2 films by electrophoretic deposition time. Thin Solid Films 515:3402–3413

Martínez C, Vilariño S, Fernández MI, Faria J, Canle ML, Santaballa JA (2013) Mechanism of degradation of ketoprofen by heterogeneous photocatalysis in aqueous solution. Appl Catal B Environ 142–143:633–646

Miller EL, Marsen B, Cole B, Lum M (2006) Low temperature reactively-sputtered tungsten oxide films for solar-powered water splitting applications. Electrochem Solid-State Lett 9:G248–G250

Miraghaei S, Santamaria M, Di Quarto F (2014) Red shift in the light absorption threshold of anodic TiO_2 films induced by nitrogen incorporation. Electrochim Acta 134:150–158

Neppolian B, Choi HC, Sakthivel S, Arabindoo B, Murugesan V (2002) Solar/UV-induced photocatalytic degradation of three commercial textile dyes. J Hazard Mater 89:303–317

Panida P, Ammathnadu SA, Xiaojun H, Richard JB, Christoph W, Stephen D (2009) Improved photoreaction yields for soft ultraviolet photolithography in organothiol self-assembled monolayers. J Phys Chem C 113:21642–21647

Pelizzetti E, Minero C, Pramauro E (1992) Photocatalytic process for destruction of organic chemicals. In: de Lasa H, Dogu G, Ravella A (eds) Chemical reactor technology for environmentally safe reactors and products. Kluwer Academic Publishers, The Netherlands, pp 557–608

Piskorski K, Przewlocki HM (2009) LPT and SLPT measurement methods o flat-band voltage (VFB) in MOS devices. J Telecomm Infor Tech 1(4):76–82

Radecka M, Rekas M, Trenczek-Zajac A, Zakrzewska K (2008) Importance of the band gap energy and flat band potential for application of modified TiO_2 photoanodes in water photolysis. J Power Sources 181(1):46–55

Rajeshwar K (2002) Fundamentals of semiconductor electrochemistry and photoelectrochemistry. Encyclopedia of electrochemistry, vol 6, 1. John Wiley & Sons, New York, pp 1–52. ISBN ISBN: 978-3-527-30398-4

Rajeshwar K, Ibañez J (1997) Environmental electrochemistry: Fundamentals and applications in pollution abatement. Academic, San Diego, 723

Reyes-Gil K, Wiggenhorn C, Brunschwing BS, Lewis NS (2013) Comparison between the quantum yields of compact and porous WO_3photoanodes. J Phys Chem C 117:14947–14957

Roy AM, De GC, Sasmal N, Bhattacharyya SS (1995) Determination of the flatband potential of semiconductor particles in suspension by photovoltage measurement. Intern J Hydrogen Energy 20(8):627–630

Sato N (1998) Electrochemistry at Metal and Semiconductor Electrodes. Elsevier Science. Print Book ISBN: 9780444828064

Schiettekatte F, Chicoine M, Forster JS, Geiger JS, Gujrathi S, Kolarova R, Paradis A, Roorda S, Wei P (2004) ERD, 15N external beam for NRRA in air, HIRBS: ion beam analysis developments on the HVEC EN-1 Tandem. Nucl Instr Meth Phys Res B 219–220:430–434

Serpone N, Pelizzetti E (1989) Photocatalysis: fundamentals and applications. John Wiley & Sons, New York, pp 135–136

Serpone N, Salinaro A (1999) Terminology, relative photonic efficiencies and quantum yields in heterogeneous photocatalysis. Part I: Suggested protocol. Pure Appl Chem 71:303–320

Serrano B, De Lasa H (1997) Photocatalytic degradation of water organic pollutants. Kinetic modeling and energy efficiency. Ind Eng Chem Res 36:4705–4711

Södergren S, Hagfeldt A, Olsson J, Lindquist SE (1994) Theoretical models for the action spectrum and the current-voltage characteristics of microporous semiconductor films in photoelectrochemical cells. J Phys Chem 98:5552–5556

Souza FL, Pimenta Lopes K, Longo E, Leite ER (2009) The influence of the film thickness of nanostructured alpha-Fe_2O_3 on water photooxidation. Phys Chem Chem Phys 11(8):1215–1219

Subramanian V, Wolf EE, Kamat PV (2004) Catalysis with TiO_2/gold nanocomposites. Effect of metal particle size on the Fermi level equilibration. J Am Chem Soc 126(15):4943–4950

Sun L, Bolton JR (1996) Determination of the quantum yield for the photochemical generation of hydroxyl radicals in TiO_2 suspensions. J Phys Chem 100:4127–4134

Tacca A, Meda L, Marra G, Savoini A, Caramori S, Cristino V, Bignozzi CA, Gonzalez-Pedro V, Boix PP, Gimenez S, Bisquert J (2012) Photoanodes based on nanostructured WO_3 for water splitting. Chem Phys Chem 13:3025–3034

Takahashi K (1979) Etch pit pattern of GaAs crystals made by light irradiated electrolytic etching. Jpn J Appl Phys 18:1741–1746

Tenne R, Hodes G (1980) Improved efficiency of CdSe photoanodes by photoelectrochemical etching. Appl Phys Lett 37:428–430

Terezo AJ, Bisquert J, Pereira EC, García-Belmonte G (2001) Separation of transport, charge storage and reaction processes of porous electrocatalytic IrO_2 and IrO_2/Nb_2O_5 electrodes. J Electroanal Chem 508:59–69

Thornton JM, Raftery D (2012) Efficient photocatalytic hydrogen production by platinum-loaded carbon-doped cadmium indate nanoparticles. ACS Appl Mater Interfaces 4:2426–2431

Turchi CS, Ollis DF (1990) Photocatalytic degradation of organic water contaminants: mechanisms involving hydroxyl radical attack. J Cat 122:178–192

Vanmaekelbergh D, de Jongh PE (1999) Driving force for electron transport in porous nanostructured photoelectrodes. J Phys Chem B 103:747–750

Wang CM, Heller A, Gerischer H (1992) Palladium catalysis of O_2 reduction by electrons accumulated on TiO_2 particles during photoassisted oxidation of organic compounds. J Am Chem Soc 114:5230–5234

Wang C, Pagel R, Bahnemann DW, Dohrmann JK (2004) Quantum yields of formaldehyde formation in the presence of colloidal TiO2-based photocatalysts: effect of intermittent illumination, platinization, and deoxygenation. J Phys Chem B 108:14082–14092

Yan G, Zhang M, Houa J, Yang J (2011) Photoelectrochemical and photocatalytic properties of N + S co-doped TiO2 nanotube array films under visible light irradiation. Mater Chem Phys 129(1–2):553–557

Yu JG, Yu HG, Cheng B, Zhao XJ, Yu JC, Ho WK (2003) The effect of calcination temperature on the surface microstructure and photocatalytic activity of TiO_2 thin films prepared by liquid phase deposition. J Phys Chem B 107:13871–13879

Zhang L, Yu JC (2003) A sonochemical approach to hierarchical porous titania spheres with enhanced photocatalytic activity. Chem Commun 2003:2078–2079